

Triaxiality Dependence of Octupole Excitations on Superdeformed States in ^{44}Ti

Hiromichi OGASAWARA,¹ Kenichi YOSHIDA,² Masayuki YAMAGAMI,²
Shoujiro MIZUTORI³ and Kenichi MATSUYANAGI²

¹*Department of Physics, Graduate School of Science, Kyoto University,
Kyoto 606-8502, Japan*

²*Theoretical Nuclear Physics Laboratory, RIKEN Nishina Center,
Wako 351-0198, Japan*

³*Department of Human Science, Kansai Women's College, Osaka 582-0026, Japan*

(Received September 1, 2008)

By random phase approximation (RPA) calculation based on triaxially deformed Woods-Saxon potential, we investigate how axial-symmetry breaking in the mean field affects the properties of octupole vibrational excitations built on superdeformed states in ^{44}Ti . We find a remarkable dependence of their properties on signature quantum number with respect to rotation about an axis perpendicular to the longest axis by the angle of π . Detailed numerical analysis of the signature dependence is made by considering the magnitude of the triaxial deformation γ as a parameter.

§1. Introduction

In the last two decades, more than two hundred superdeformed (SD) bands have been found in various mass regions.^{1)–5)} The SD shell structure is significantly different from that of normal deformation; each major shell at the SD shape consists of about equal numbers of positive- and negative-parity levels. This is a favourable situation for the appearance of negative-parity collective modes. In fact, various mean-field calculations^{6)–9)} and random phase approximation (RPA) calculations^{10),11)} based on the rotating mean field (cranked shell model) indicated that SD nuclei are very soft against both the axial and nonaxial octupole deformations. Thus, low-frequency soft octupole vibrations were predicted to appear near the SD yrast lines,^{12),13)} and identified in experiments for SD states in the Hg-Pb region,^{14),15)} and in ^{152}Dy .¹⁶⁾

In recent years, the SD bands have been discovered also in the ^{40}Ca region: the rotational band built on the excited 0^+ state at about 5.2 MeV in ^{40}Ca was found to be superdeformed.^{17),18)} The rotational band built on the excited 0^+ state at about 1.9 MeV in ^{44}Ti may also be regarded as belonging to a family of the SD band.¹⁹⁾ In view of the fact that the low-angular-momentum portions of the SD bands in heavy nuclei are unknown in almost all cases (except the fission isomers), the observation of rotational bands starting from the 0^+ states is a unique feature characterizing the SD states in the ^{40}Ca region. It was then confirmed that symmetry-unrestricted Skyrme-Hartree-Fock (SHF) calculation indeed yields the SD local minima corresponding to these experimental data.²⁰⁾ Thus, it has become clear nowadays that even the doubly magic nucleus in the spherical shell model, like ^{40}Ca , can easily take a strongly

deformed shape if it is given excitation energy of only about 5 MeV. One of the significances of this type of phenomenon is that it exhibits the ability of the nucleus to take quite different microscopic structures with almost the same binding energy, and these different structures can coexist while retaining their identities.

The investigation of low-frequency octupole vibrations built on the SD states in the $A = 30$ – 50 region showed some new features that are absent in the study of heavy SD nuclei. For the $N = Z$ nuclei in the ^{40}Ca region, it may be possible to observe in experiment such collective modes built on the known SD 0^+ states. Moreover, because the proton and neutron shell structures are essentially the same, we can expect that strong coherence takes place between the proton and neutron excitations and brings about an enhanced collectivity of these modes. Thus, Inakura et al.²¹⁾ theoretically explored such a possibility by means of the mixed-representation RPA^{22),23)} based on the SHF mean field, and suggested the appearance of low-frequency negative-parity collective modes possessing strongly enhanced isoscalar octupole transition strengths. In this region of nuclear chart, the number of particle-hole configurations is smaller than those in heavier nuclei. This might be an unfavorable situation to generate vibrational collectivity by coherent superposition of a large number of particle-hole excitations. On the other hand, it provides a unique situation to make a detailed microscopic analysis of how collective modes emerge out of a relatively small number of particle-hole configurations. Thus we can learn the similarity and difference of octupole vibrations built on SD states in various mass regions. The mixed-representation RPA calculation in Ref. 21) is fully self-consistent in the sense that the same effective interaction is used in both the mean-field and RPA calculations. On the other hand, it is not easy in this approach to identify microscopic particle-hole configurations generating individual RPA modes. Therefore, with the use of deformed Woods-Saxon potential and the conventional matrix formulation of the RPA, Yoshida et al.²⁴⁾ carried out a detailed analysis of the microscopic structure of octupole excitation modes built on the SD states in ^{40}Ca and other nuclei. In that work, however, the single-particle Hamiltonian was solved in terms of the two-dimensional mesh representation with cylindrical coordinate system. Thus, the mean field was restricted to axially symmetric shapes.

In this paper, we extend the previous work²⁴⁾ so as to allow for the breaking of axial symmetry in the mean field. For this purpose, we construct a new computer code to solve the triaxially deformed Woods-Saxon potential in terms of the three-dimensional Cartesian coordinate system. On the single-particle basis thus obtained, we carry out RPA calculation diagonalizing the RPA matrix. Our major purpose is to investigate the effects of the triaxial deformation of the mean field on the properties of octupole vibrations built on SD states. As a typical example, we take up the case of ^{44}Ti where experimental data is available for a candidate of the SD yrast state¹⁹⁾ and a sizable triaxial deformation is predicted in SHF calculations.^{20),21)} The magnitude of the calculated triaxial deformation parameter γ depends on the version of the Skyrme interaction and takes the values in the range 7° – 18° . In the present paper, we consider γ as a parameter and make a detailed analysis of how axial-symmetry breaking in the mean field affects the properties of octupole vibrational excitations built on the SD state in ^{44}Ti . We find a remarkable dependence of their properties

on signature quantum number with respect to rotation about the intermediate axis by the angle of π .

This paper is organized as follows. In §2, the properties of single-particle wave functions in triaxially deformed potential are recapitulated. In §3, the RPA scheme for octupole vibrational excitations on the triaxially deformed mean field is summarized, with special attention on their symmetry properties with respect to reflections about the (x, y) -, (y, z) -, and (z, x) -planes. In §4, results of numerical analysis of octupole excitations built on the SD state in ^{44}Ti are presented. In §5, concluding remarks are given.

§2. Triaxially deformed mean field

2.1. Single-particle Hamiltonian

We write nucleon creation and annihilation operators in a single-particle state k as \hat{c}_k^\dagger and \hat{c}_k . With the use of the two-component single-particle wave function $\varphi_k(\vec{r})$ consisting of spin-up and spin-down components with respect to the z -axis, nucleon creation and annihilation operators at a spatial position \vec{r} are then represented as

$$\hat{\psi}^\dagger(\vec{r}) = \sum_k \varphi_k^\dagger(\vec{r}) \hat{c}_k^\dagger = \sum_k (\varphi_{k\uparrow}^*(\vec{r}), \varphi_{k\downarrow}^*(\vec{r})) \hat{c}_k^\dagger, \quad (2.1)$$

$$\hat{\psi}(\vec{r}) = \sum_k \varphi_k(\vec{r}) \hat{c}_k = \sum_k \begin{pmatrix} \varphi_{k\uparrow}(\vec{r}) \\ \varphi_{k\downarrow}(\vec{r}) \end{pmatrix} \hat{c}_k. \quad (2.2)$$

We use a mean-field potential consisting of an axially asymmetric Woods-Saxon potential $V_{\text{WS}}(\vec{r})$ and a spin-orbit potential $V_{\text{so}}(\vec{r}, \vec{\nabla})$. In terms of the field operators defined above, the single-particle Hamiltonian is then written as

$$\hat{h} = \int \hat{\psi}^\dagger(\vec{r}) h(\vec{r}, \vec{\nabla}) \hat{\psi}(\vec{r}) d^3\vec{r}, \quad (2.3)$$

$$h(\vec{r}, \vec{\nabla}) = \left[-\frac{\hbar^2}{2m} \Delta + V_{\text{WS}}(\vec{r}) \right] \mathbf{1} + V_{\text{so}}(\vec{r}, \vec{\nabla}), \quad (2.4)$$

where $\mathbf{1}$ denotes the unit matrix in the 2×2 spin space. Explicit expressions of the Woods-Saxon and spin-orbit potentials are

$$V_{\text{WS}}(\vec{r}) = -V_0 [1 + \exp((r - R(\theta, \phi))/a)]^{-1}, \quad (2.5)$$

$$V_{\text{so}}(\vec{r}, \vec{\nabla}) = \frac{i\hbar^2 q}{2} \left[\frac{\partial V_{\text{WS}}(\vec{r})}{\partial \vec{r}} \times \vec{\sigma} \right] \cdot \vec{\nabla}, \quad (2.6)$$

where a is the diffuseness parameter and

$$R(\theta, \phi) = R_0(\beta, \gamma) \left(1 + \beta \cos \gamma Y_{2,0}(\theta, \phi) + \frac{1}{\sqrt{2}} \beta \sin \gamma (Y_{2,+2}(\theta, \phi) + Y_{2,-2}(\theta, \phi)) \right). \quad (2.7)$$

The deformation parameters, β and γ , indicate the magnitude of quadrupole deformation and its triaxiality, respectively. In this parametrization of nuclear surface,

when $\beta > 0$, at $\gamma = 0^\circ$, the potential is symmetric about the z -axis, which is the longest principal axis (prolate shape). With increasing value of γ , the potential extends in the direction of the x -axis, and becomes at $\gamma = 60^\circ$ symmetric about the y -axis, which is the shortest principal axis (oblate shape). Although an angle-dependent diffuseness parameter $a(\theta, \phi)$ is better for accurate calculation,²⁵⁾ we use a constant a for simplicity.

The effective spherical radius $R_0(\beta, \gamma)$ is fixed under the condition that the volume enclosed by $R(\theta, \phi)$ takes the constant value $\frac{4}{3}\pi r_0^3 A$, A being the mass number. Its explicit expression is

$$R_0(\beta, \gamma) = r_0 A^{1/3} \left(1 + \frac{3}{4\pi} \beta^2 + \frac{\sqrt{5}}{28\pi\sqrt{\pi}} \beta^3 \cos 3\gamma \right)^{-1/3}. \quad (2.8)$$

In the numerical calculation, we use the parameters shown in Ref. 28) for the $N = Z$ case, i.e., $V_0 = 51$ MeV, $\hbar^2 q = -0.44r_0^2$, $r_0 = 1.27$ fm, and $a = 0.67$ fm.

2.2. Symmetry properties of single-particle wave functions

The single-particle Hamiltonian $h(\vec{r}, \vec{\nabla})$, the parity transformation \mathcal{P} , and the rotation about the z -axis by the angle of π , $\mathcal{R}_z = e^{i\pi j_z/\hbar}$, commutes with each other: i.e., $[h(\vec{r}, \vec{\nabla}), \mathcal{P}] = 0$, $[h(\vec{r}, \vec{\nabla}), \mathcal{R}_z] = 0$, and $[\mathcal{P}, \mathcal{R}_z] = 0$. Accordingly, we can adopt single-particle wave functions $\varphi_k(\vec{r})$ that are simultaneous eigenvectors of these operators:

$$h(\vec{r}, \vec{\nabla})\varphi_k(\vec{r}) = \varepsilon_k \varphi_k(\vec{r}), \quad (2.9)$$

$$\mathcal{P}\varphi_k(\vec{r}) = p_k \varphi_k(\vec{r}), \quad (2.10)$$

$$\mathcal{R}_z \varphi_k(\vec{r}) = \alpha_k \varphi_k(\vec{r}). \quad (2.11)$$

The quantum number α_k is called z -signature and takes values $\alpha_k = \pm i$. Thus, the single-particle wave functions $\varphi_k(\vec{r})$ are specified by parity p_k and z -signature as well as single-particle energy ε_k . In fact, the single-particle Hamiltonian $h(\vec{r}, \vec{\nabla})$ commutes with $\mathcal{R}_x = e^{i\pi j_x/\hbar}$ and also with $\mathcal{R}_y = e^{i\pi j_y/\hbar}$, as well as \mathcal{R}_z . Therefore, we can adopt x -signature or y -signature in place of z -signature to specify single-particle wave functions. It is, however, convenient to use the z -signature when we adopt the z -axis as a quantization axis of spin. In this case, the spin-up and spin-down components of the wave function in Eq. (2.2) satisfy the following symmetry properties with respect to reflections about the (y, z) -, (z, x) -, and (x, y) -planes (see Appendix A):^{26),27)}

$$\varphi_{k\sigma}(-x, y, z) = -i\alpha_k \sigma \varphi_{k\sigma}^*(x, y, z), \quad (2.12)$$

$$\varphi_{k\sigma}(x, -y, z) = \varphi_{k\sigma}^*(x, y, z), \quad (2.13)$$

$$\varphi_{k\sigma}(x, y, -z) = -ip_k \alpha_k \sigma \varphi_{k\sigma}(x, y, z), \quad (2.14)$$

where $\sigma = +1$ and -1 for spin-up \uparrow and spin-down \downarrow , respectively. The single-particle Hamiltonian $h(\vec{r}, \vec{\nabla})$ is also invariant with respect to time reversal $\mathcal{T} = i\sigma_y \mathcal{K}$, where \mathcal{K} denotes operation of taking the complex conjugate of all c -numbers, and

the phase convention of Bohr-Mottelson²⁸⁾ is adopted. Operating \mathcal{T} on both sides of the Schrödinger equation (2.9), we readily see that the time-reversal partner $\mathcal{T}\varphi_k(\vec{r})$ possesses the z -signature quantum number $\alpha_k^* = -\alpha_k$. Thus, there is a one-to-one correspondence between a time-reversal partner and a z -signature partner. Thanks to this property, we need to diagonalize the single-particle Hamiltonian only for the $\alpha = +i$ sector or the $\alpha = -i$ sector. Single-particle wave functions having opposite z -signatures are then immediately obtained as time-reversal partners of these eigenfunctions.

In diagonalizing the single-particle Hamiltonian, we use, instead of the well-known harmonic-oscillator basis, three-dimensional Cartesian coordinate mesh representation with box boundary condition.^{26),27)} As discussed in Refs. 26) and 27), we need to explicitly consider only the octant region in space with $x \geq 0$, $y \geq 0$, and $z \geq 0$, owing to the reflection symmetries (2.12)–(2.14).

The major reason why we use the coordinate mesh representation is that we intend to apply, in due course, the present approach to neutron-rich unstable nuclei close to the drip line where the continuum plays an essential role and the coordinate mesh representation is better suited for this aim. We also intend to replace, in the future, the Woods-Saxon potential with the SHF potential. The computer program constructed in this work will serve as a first step toward such self-consistent mean-field approach.

In the numerical calculation, we take the box size extending about 2.5 times of the radius $R(\theta, \phi)$ in each direction and the space is discretized with the mesh spacing 0.6 fm. Numerical reliability with respect to the box size and the mesh spacing was carefully checked by Inakura et al.²¹⁾ and shown that this choice gives fairly accurate results. Specifically, we take 17, 17, and 25 lattice points in the x -, y -, and z -direction, respectively, for the region of the triaxiality parameter $0^\circ \leq \gamma \leq 4^\circ$. These numbers are 17, 15, and 25 (19, 15, and 25) for $6^\circ \leq \gamma \leq 16^\circ$ ($18^\circ \leq \gamma \leq 30^\circ$). For the nucleus ^{44}Ti with $N = Z$, we use the same single-particle wave functions for protons and neutrons ignoring the Coulomb potential.

§3. RPA for octupole vibrations in triaxially deformed nuclei

3.1. Eigenvalue equations

Introducing a residual interaction \hat{v} , we solve the RPA eigenvalue equation for the total Hamiltonian $\hat{H} = \hat{h} + \hat{v}$ with

$$\hat{v} = \frac{1}{2} \sum_{\substack{k_1, k_2 \\ k'_1, k'_2}} v_{k'_1 k'_2 k_1 k_2} \hat{c}_{k'_2}^\dagger \hat{c}_{k'_1}^\dagger \hat{c}_{k_1} \hat{c}_{k_2}, \quad (3.1)$$

$$v_{k'_1 k'_2 k_1 k_2} = \sum_{\substack{\sigma_1, \sigma_2 \\ \sigma'_1, \sigma'_2}} \iint \varphi_{k'_1 \sigma'_1}^*(\vec{r}_1) \varphi_{k'_2 \sigma'_2}^*(\vec{r}_2) v_{\sigma_1 \sigma_1 \sigma'_2 \sigma_2}(\vec{r}_1, \vec{r}_2) \varphi_{k_1 \sigma_1}(\vec{r}_1) \varphi_{k_2 \sigma_2}(\vec{r}_2) d^3 \vec{r}_1 d^3 \vec{r}_2. \quad (3.2)$$

Specifically, we use a density-dependent contact interaction of the following form:²⁹⁾

$$v_{\sigma_1 \sigma_1 \sigma'_2 \sigma_2}(\vec{r}_1, \vec{r}_2) = \left\{ \left[t_0 + \frac{1}{6} t_3 \rho(\vec{r}_1) \right] \delta_{\sigma_1 \sigma'_1} \delta_{\sigma_2 \sigma'_2} \right.$$

$$+ \left[t_0 x_0 + \frac{1}{6} t_3 x_3 \rho(\vec{r}_1) \right] \delta_{\sigma_1 \sigma'_2} \delta_{\sigma_2 \sigma'_1} \left. \right\} \delta^3(\vec{r}_1 - \vec{r}_2). \quad (3.3)$$

Here, $\rho(\vec{r})$ is the nucleon density. For the interaction parameters t_0 , t_3 , x_0 , and x_3 , we use the same values as in Shlomo-Bertsch:²⁹⁾ $t_0 = -1100 \text{ MeV}\cdot\text{fm}^3$, $t_3 = 16000 \text{ MeV}\cdot\text{fm}^6$, $x_0 = 0.5$, and $x_3 = 1.0$.

We now introduce the particle-hole concept. The single-particle states above the Fermi energy ε_F is called *particle states* and those below ε_F is called *hole states*. The *particle* creation and annihilation operators ($\hat{a}_k^\dagger, \hat{a}_k$) and the *hole* creation and annihilation operators ($\hat{b}_k^\dagger, \hat{b}_k$) are defined as

$$\hat{c}_k^\dagger = (1 - \theta_k) \hat{a}_k^\dagger + \theta_k \hat{b}_k, \quad (3.4)$$

$$\hat{c}_k = (1 - \theta_k) \hat{a}_k + \theta_k \hat{b}_k^\dagger, \quad (3.5)$$

where θ_k is the occupation number defined as

$$\theta_k = \begin{cases} 1 & \text{for } \varepsilon_k \leq \varepsilon_F, \\ 0 & \text{for } \varepsilon_k > \varepsilon_F. \end{cases} \quad (3.6)$$

The creation operators of the RPA eigenmodes are written as

$$\hat{X}_n^\dagger = \sum_{p,h} (f_{ph}^n \hat{a}_p^\dagger \hat{b}_h^\dagger - g_{ph}^n \hat{b}_h \hat{a}_p). \quad (3.7)$$

From now on, we use the index p (h) to specify the particle (hole) states and keep the index k for general cases. As usual, from the linearized equation of motion,

$$[\hat{H}, \hat{X}_n^\dagger] = \hbar\omega_n \hat{X}_n^\dagger, \quad (3.8)$$

we obtain eigenvalue equations in matrix form

$$\sum_{p'h'} \begin{pmatrix} A_{php'h'} & B_{php'h'} \\ -B_{php'h'}^* & -A_{php'h'}^* \end{pmatrix} \begin{pmatrix} f_{p'h'}^n \\ g_{p'h'}^n \end{pmatrix} = \hbar\omega_n \begin{pmatrix} f_{ph}^n \\ g_{ph}^n \end{pmatrix} \quad (3.9)$$

for each sector specified by parity p and z -signature α . The matrix elements $A_{php'h'}$ and $B_{php'h'}$ are given as

$$A_{php'h'} = (\varepsilon_p - \varepsilon_h) \delta_{pp'} \delta_{hh'} + \bar{v}_{ph'hp'}, \quad B_{php'h'} = \bar{v}_{pp'hh'}, \quad (3.10)$$

where $\bar{v}_{k'_1 k'_2 k_1 k_2} = v_{k'_1 k'_2 k_1 k_2}$ when (k_1, k_2) are between a proton and a neutron (vice versa) while $\bar{v}_{k'_1 k'_2 k_1 k_2} = v_{k'_1 k'_2 k_1 k_2} - v_{k'_2 k'_1 k_1 k_2}$ taking both combinations (k_1, k'_1) and (k_2, k'_2) when (k_1, k_2) are identical nucleons. In the numerical calculation, we take into account all the particle-hole pairs with $\varepsilon_p - \varepsilon_h \leq 30 \text{ MeV}$.

3.2. Octupole transition amplitudes

For any one-body operator

$$\hat{O} = \sum_{k,k'} O_{k'k} \hat{c}_{k'}^\dagger \hat{c}_k \quad \text{with} \quad O_{k'k} = \int \varphi_{k'}^\dagger(\vec{r}) O(\vec{r}) \varphi_k(\vec{r}) d^3\vec{r}, \quad (3.11)$$

Table I. Octupole operators classified according to z -component K and x -signature ξ .

	$\xi = +1$	$\xi = -1$
$K = 0$		$\sqrt{\frac{7}{16\pi}} \{2z^2 - 3(x^2 + y^2)\} z$
$K = 1$	$\sqrt{\frac{21}{32\pi}} \{4z^2 - (x^2 + y^2)\} x$	$\sqrt{\frac{21}{32\pi}} \{4z^2 - (x^2 + y^2)\} y$
$K = 2$	$\sqrt{\frac{105}{4\pi}} xyz$	$\sqrt{\frac{105}{16\pi}} (x^2 - y^2) z$
$K = 3$	$\sqrt{\frac{35}{32\pi}} (x^2 - 3y^2) x$	$\sqrt{\frac{35}{32\pi}} (3x^2 - y^2) y$

transition amplitudes between the RPA ground state $|0\rangle$ and excited states $|n\rangle = \hat{X}_n^\dagger|0\rangle$ are evaluated as

$$\langle 0|\hat{O}|n\rangle = \langle 0|[\hat{O}, \hat{X}_n^\dagger]|0\rangle = \sum_{p,h} (O_{hp}f_{ph}^n + O_{ph}g_{ph}^n). \tag{3.12}$$

In this paper, we focus our attention on octupole transition strengths. It is then convenient to classify the octupole operators according to z -component K of its angular momentum and x -signature ξ representing symmetry property for rotation π about the x -axis:

$$\mathcal{R}_x O^{(K,\xi)}(\vec{r}) \mathcal{R}_x^{-1} = \xi O^{(K,\xi)}(\vec{r}) \quad \text{for} \quad \mathcal{R}_x = e^{i\pi j_x/\hbar}. \tag{3.13}$$

In terms of the spherical coordinates (r, θ, ϕ) , they are given as

$$O^{(0,-)}(\vec{r}) = r^3 Y_{3,0}(\theta, \phi) \quad \text{for} \quad K = 0, \tag{3.14}$$

$$O^{(K,+)}(\vec{r}) = \frac{i}{\sqrt{2}} r^3 [Y_{3,-K}(\theta, \phi) - (-1)^K Y_{3,+K}(\theta, \phi)] \quad \text{for} \quad K \neq 0, \tag{3.15}$$

$$O^{(K,-)}(\vec{r}) = \frac{1}{\sqrt{2}} r^3 [Y_{3,-K}(\theta, \phi) + (-1)^K Y_{3,+K}(\theta, \phi)] \quad \text{for} \quad K \neq 0. \tag{3.16}$$

In this classification, $O^{(K,\xi)}(\vec{r})$ are real functions; their explicit expressions in terms of the Cartesian coordinates are listed in Table I. We note that the octupole operators with odd- K (even- K) values have z -signature $\alpha = -1$ ($+1$), which follows from the transformation property for rotation about the z -axis by the angle of π :

$$\mathcal{R}_z O^{(K,\xi)}(\vec{r}) \mathcal{R}_z^{-1} = (-1)^K O^{(K,\xi)}(\vec{r}). \tag{3.17}$$

3.3. Symmetry for rotation about the x -axis by angle of π (x -signature)

The single-particle Hamiltonian $h(\vec{r}, \vec{\nabla})$ commutes with \mathcal{R}_x and \mathcal{R}_z individually but the commutator between \mathcal{R}_x and \mathcal{R}_z is nonzero, so that it is impossible to construct a single-particle basis spanned by simultaneous eigenstates of x - and z -signatures. In contrast, creation and annihilation operators of the RPA eigenmodes \hat{X}_n^\dagger and \hat{X}_n , carry definite x - and z -signatures simultaneously. We can examine this fact in the following manner. First, we can prove that the A and B matrix elements associated with z -signature partners are identical; $A_{\bar{p}\bar{h}\bar{p}'\bar{h}'} = A_{php'h'}$ and $B_{\bar{p}\bar{h}\bar{p}'\bar{h}'} = B_{php'h'}$ (see Appendix B). It immediately follows that the RPA particle-hole amplitudes of z -signature partners differ at most by sign, i.e., $(f_{\bar{p}\bar{h}}^n, g_{\bar{p}\bar{h}}^n) = \pm(f_{ph}^n, g_{ph}^n)$.

Next, let us evaluate transition matrix elements of the octupole operators with definite x - and z -signatures $\hat{O}^{(K,\xi)}$ between RPA excited states and the ground state (recall that z -signature $\alpha = (-1)^K$). They are calculated as

$$\begin{aligned} \langle 0 | \hat{O}^{(K,\xi)} | n \rangle &= \sum_{p,h} (O_{ph}^{(K,\xi)*} f_{ph}^n + O_{ph}^{(K,\xi)} g_{ph}^n) \\ &= \sum'_{p,h} (O_{ph}^{(K,\xi)*} f_{ph}^n + O_{\bar{p}\bar{h}}^{(K,\xi)*} f_{\bar{p}\bar{h}}^n + O_{ph}^{(K,\xi)} g_{ph}^n + O_{\bar{p}\bar{h}}^{(K,\xi)} g_{\bar{p}\bar{h}}^n) \\ &= \sum'_{p,h} \left[O_{ph}^{(K,\xi)*} (f_{ph}^n - \xi f_{\bar{p}\bar{h}}^n) + O_{ph}^{(K,\xi)} (g_{ph}^n - \xi g_{\bar{p}\bar{h}}^n) \right]. \end{aligned} \quad (3.18)$$

In the second equality above, the sum over the particle and hole states is divided into two parts consisting of z -signature partners; $\sum'_{p,h}$ denotes a summation over such signature pairs. Then, in the third equality, the relation, $O_{\bar{p}\bar{h}}^{(K,\xi)} = -\xi O_{ph}^{(K,\xi)}$, is utilized (see Appendix B). Assuming that the x -signature of the RPA ground state $|0\rangle$ is $+1$, the above expression indicates that the RPA excited states $|n\rangle$ created by \hat{X}_n^\dagger possess definite ξ values. In other words, the RPA eigenmodes whose amplitudes possess such properties as $(f_{\bar{p}\bar{h}}^n, g_{\bar{p}\bar{h}}^n) = (f_{ph}^n, g_{ph}^n)$ create excited states with $\xi = -1$, while those with $(f_{\bar{p}\bar{h}}^n, g_{\bar{p}\bar{h}}^n) = -(f_{ph}^n, g_{ph}^n)$ create excited $\xi = +1$ states.

It should be noted here that, owing to the identity $\mathcal{R}_x \mathcal{R}_y \mathcal{R}_z = \mathbf{1}$ (see Appendix B), essentially the same argument as above holds when we adopt the y -signature associated with \mathcal{R}_y (rotation about the y -axis by the angle of π) in place of the x -signature.

By taking into account the relation $O_{hp}^{(K,\xi)} = -(-1)^K \xi O_{ph}^{(K,\xi)}$ (see Appendix B) and that the proton and neutron contributions are the same for nuclei with $N = Z$ under the present approximation, the transition amplitudes for the isoscalar octupole operators with definite (K, ξ) are calculated as

$$\langle 0 | \hat{O}^{(K,\xi)} | n \rangle = 4 \sum''_{p,h} O_{ph}^{(K,\xi)} (-(-1)^K \xi f_{ph}^n + g_{ph}^n) \equiv \sum''_{p,h} M_{ph}^{(K,\xi)}, \quad (3.19)$$

where $\sum''_{p,h}$ denotes a summation over z -signature partners of protons (or neutrons).

We call the quantities $S_{3K} \equiv |\langle 0 | \hat{O}^{(K,\xi)} | n \rangle|^2$ “isoscalar octupole transition strengths” often omitting the adjective “isoscalar”. Note that these are quantities defined in the intrinsic coordinate frame and we cannot directly compare these quantities with experimental data. For this, it is necessary to construct wave functions in the laboratory frame by means of the Bohr-Mottelson approach³⁰⁾ or the angular momentum projection method.³¹⁾ This subject is left for a future work, however.

3.4. Elimination of spurious components

Owing to the rotational symmetry breaking associated with the deformed mean field, dipole excitation modes can mix with the octupole excitation modes. As is well known, in the self-consistent RPA scheme where the same microscopic Hamiltonian is used in constructing the mean field and RPA excitation modes, the lowest isoscalar

modes corresponding to the center of mass motions appear at zero energy and they are separated from other excitation modes. In our present nonself-consistent calculation, such components associated with center of mass motion may mix in the RPA solutions representing octupole vibrations of interest. It is therefore necessary to adopt some recipe to eliminate such spurious coupling effects. For this purpose, we adopt the recipe that is widely used (see, e.g., Ref. 32)). First, we multiply a common factor λ to the interaction matrix elements $v_{k'_1 k'_2 k_1 k_2}$ and determine its value so that the lowest eigenvalue of the RPA matrix becomes zero. There are three center of mass modes representing displacements in the x , y , and z directions. It is easily seen that they carry quantum numbers $(K, \xi) = (1, +1)$, $(1, -1)$, and $(0, -1)$, respectively. Therefore, we determine λ separately for the $(\alpha, \xi) = (-1, +1)$, $(-1, -1)$, and $(+1, -1)$ sectors. Note that the z -signature $\alpha = (-1)^K$ is conserved under the K -mixing owing to the triaxial deformation and that there is no spurious mode in the $(\alpha, \xi) = (+1, +1)$ sector. We can easily identify these spurious modes among the solutions of the RPA eigenvalue problem by evaluating isoscalar dipole transition amplitudes, since they have extremely large values.

If the separation of the spurious modes is perfectly carried out, the transition amplitudes of the isoscalar dipole operators $\hat{D}^{(K, \xi)}$, which are proportional to x , y , and z individually, should vanish for the octupole excited states of interest:

$$\langle 0 | \hat{D}^{(K, \xi)} | n \rangle = 0. \quad (3.20)$$

In practice, it is difficult to meet this condition owing to the small but nonnegligible mixture of the spurious component. Thus, in the next step, we remove such a mixture from the octupole excited states obtained in the RPA calculation “by hand”. Namely, we subtract the dipole component corresponding to the center of mass excitation, $\hat{D}^{(K, \xi)} | 0 \rangle$, from every RPA excited state $| n \rangle$ in each (α, ξ) sector (there is a connection between (K, ξ) and (α, ξ) as mentioned above):

$$| n \rangle \longrightarrow \mathcal{N} (| n \rangle - \chi \hat{D} | 0 \rangle) \quad \text{with} \quad \chi = \frac{\langle 0 | \hat{D} | n \rangle}{\langle 0 | \hat{D}^2 | 0 \rangle}, \quad (3.21)$$

where $\mathcal{N} = (1 - |\chi|^2 \langle 0 | \hat{D}^2 | 0 \rangle)^{-1/2}$. It is easily seen that this is equivalent to the replacement of the RPA forward and backward amplitudes, (f_{ph}^n, g_{ph}^n) , in the following manner:

For the $\alpha = -1$ sector,

$$f_{ph}^n + g_{ph}^n \longrightarrow f_{ph}^n + g_{ph}^n - \frac{\sum_{p', h'} x_{p' h'} (f_{p' h'}^n + g_{p' h'}^n)}{\sum_{p', h'} |x_{p' h'}|^2} x_{ph}^*, \quad (\xi = +1) \quad (3.22)$$

$$f_{ph}^n - g_{ph}^n \longrightarrow f_{ph}^n - g_{ph}^n - \frac{\sum_{p', h'} y_{p' h'} (f_{p' h'}^n - g_{p' h'}^n)}{\sum_{p', h'} |y_{p' h'}|^2} y_{ph}^*. \quad (\xi = -1) \quad (3.23)$$

For the $\alpha = +1$ sector,

$$f_{ph}^n + g_{ph}^n \longrightarrow f_{ph}^n + g_{ph}^n - \frac{\sum_{p', h'} z_{p' h'} (f_{p' h'}^n + g_{p' h'}^n)}{\sum_{p', h'} |z_{p' h'}|^2} z_{ph}^*, \quad (\xi = -1) \quad (3.24)$$

$$f_{ph}^n - g_{ph}^n \longrightarrow f_{ph}^n - g_{ph}^n. \quad (\xi = +1) \quad (3.25)$$

Here x_{ph} , y_{ph} , and z_{ph} represent $\langle 0|\hat{x}|ph\rangle$, $\langle 0|\hat{y}|ph\rangle$, and $\langle 0|\hat{z}|ph\rangle$, respectively. After the above replacements, we renormalize them such that new amplitudes satisfy the normalization condition $\sum_{p,h}(|f_{ph}^n|^2 - |g_{ph}^n|^2) = 1$.

§4. Numerical analysis and discussion

4.1. Dependence of single-particle energies on β and γ

Figure 1 shows the single-particle energies as functions of the deformation parameter β . We can clearly see that the shell gap at $N = Z = 20$ at the superdeformed shape with $\beta \simeq 0.6-0.7$ is responsible for the superdeformed excited state in ^{40}Ca . For ^{44}Ti with $N = Z = 22$, the superdeformed minimum obtained in the SHF calculation^{20),21)} corresponds to the relatively small shell gap at $\beta \simeq 0.5$.

In Fig. 2, single-particle energies are plotted as functions of the triaxiality parameter γ fixing β at 0.5. It is seen that the shell gap at $N = Z = 22$ slightly increases with increasing γ indicating that the triaxial deformation is favoured but the effect is not very strong. This property of the single-particle diagram suggests the triaxial minimum of the mean field is rather soft with respect to the γ degree of

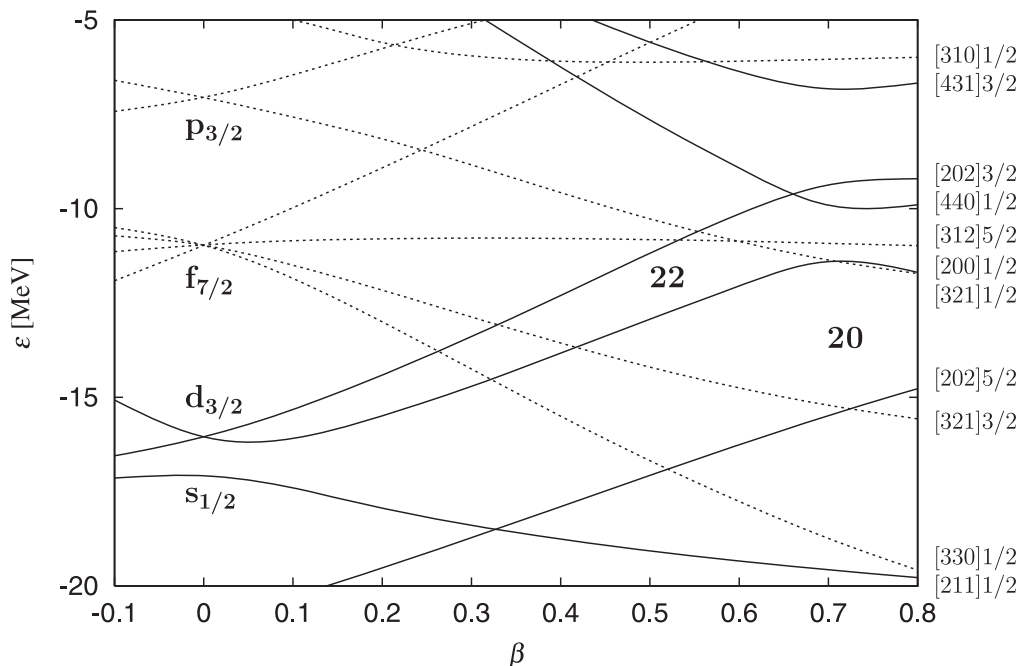


Fig. 1. Single-particle energies ε in the $N = Z$ nucleus ^{44}Ti for the Woods-Saxon plus spin-orbit potentials of Eq. (2.4) plotted as functions of the deformation parameter β . Positive and negative parity levels are indicated by solid and dotted lines, respectively. For convenience, they are labelled in the region of large β by asymptotic quantum numbers indicating the largest components at $\beta \simeq 0.5$ and connected adiabatically through the level crossing region. These single-particle energies are used for both protons and neutrons.

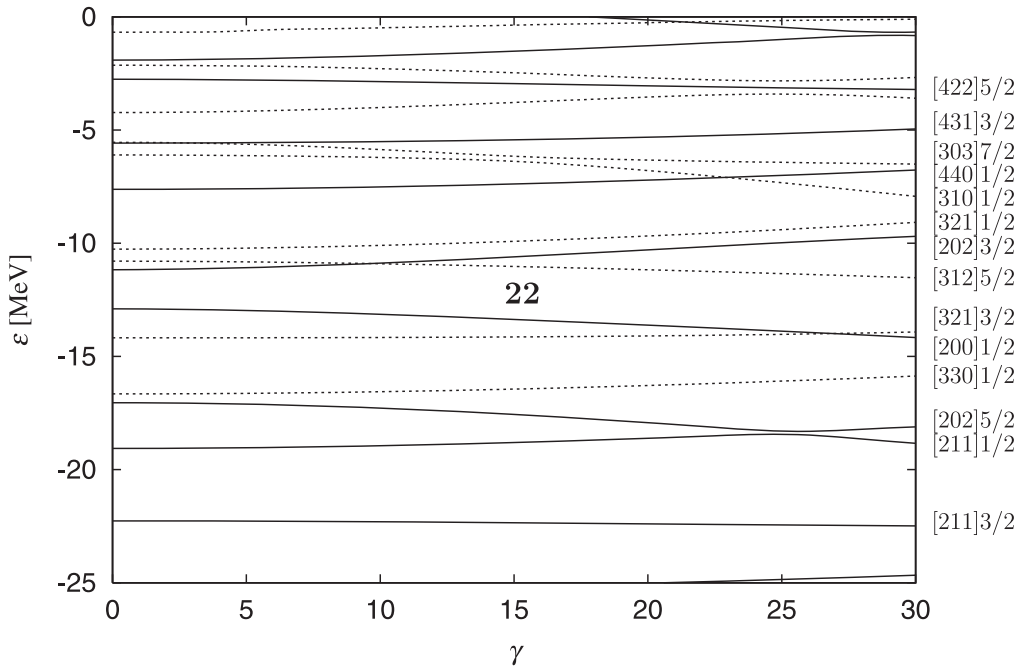


Fig. 2. Dependence of single-particle energies ε on the triaxiality parameter γ . The β is fixed at 0.5. Positive and negative parity levels are indicated by solid and dotted lines, respectively. For convenience, they are labelled with asymptotic quantum numbers indicating the largest components at the prolate limit ($\gamma = 0^\circ$) and connected adiabatically for variation of γ .

freedom. In such a situation, large-amplitude vibrational motions in this direction may take place, and it would be necessary to consider γ as a dynamical variable. This challenging subject is beyond the scope of the present paper, however. Below, we investigate the properties of octupole excitation modes built on the SD state in ^{44}Ti considering γ as a parameter. We discuss the $\alpha = \pm 1$ sectors separately.

4.2. Interplay of $K = 1$ and 3 components in the $\alpha = -1$ sector

In Fig. 3, we show the excitation energies and transition strengths S_{31} ($K = 1$) of low-lying RPA octupole excitation modes with negative z -signature ($\alpha = -1$) built on a superdeformed state in ^{44}Ti as functions of the triaxiality parameter γ . In the prolate limit ($\gamma = 0^\circ$), the z -component of angular momentum K ($= 1$ or 3) is a good quantum number and the x -signature pairs ($\xi = \pm 1$) are degenerate in energy. In this figure, the first and second excited states have $K = 3$. Their S_{33} values are small indicating their noncollective character. In contrast, the third excited state has $K = 1$ and fairly large value of S_{31} , indicating its collective character. With increasing γ , the mixing between the $K = 1$ and $K = 3$ modes takes place, the doublets split in energy, and transition strengths become different between the x -signature partners. Let us call these properties “ x -signature splitting” and “ x -signature dependence”. In Fig. 3, we see that the first and third $\xi = +1$ modes have larger S_{31} values than their signature partners $\xi = -1$. In particular, we see a

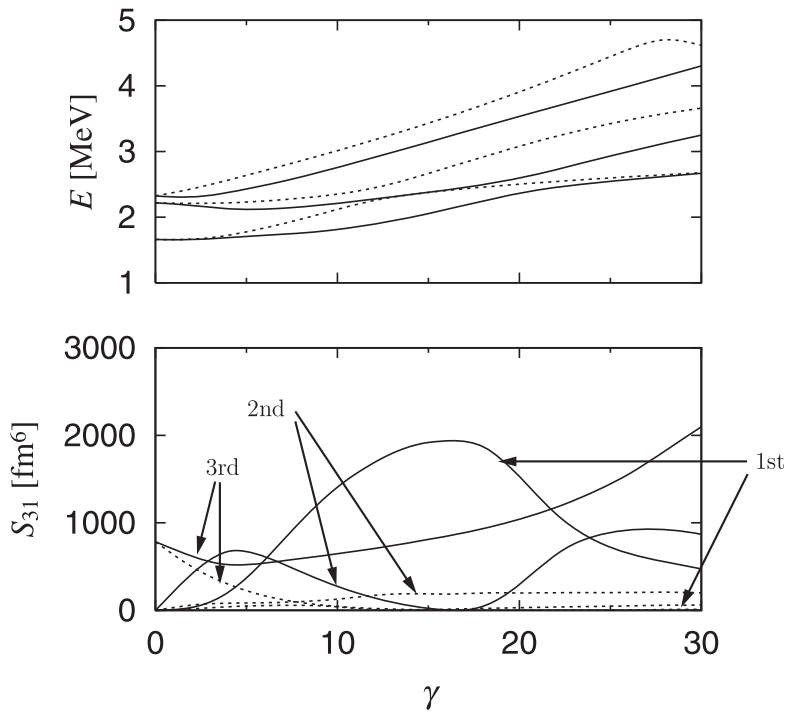


Fig. 3. Dependence on the triaxiality parameter γ of the RPA excitation energies (upper panel) and octupole transition strengths S_{31} ($K = 1$) (lower panel), calculated for octupole excitation modes with negative z -signature ($\alpha = -1$) built on a superdeformed state in ^{44}Ti . The β is fixed at 0.5. Modes with positive x -signature ($\xi = +1$) are indicated by solid lines, while those with negative x -signature ($\xi = -1$) by dotted lines. Only the lowest three x -signature pairs are presented. Octupole transition strengths S_{33} ($K = 3$) are not shown because they are very small.

remarkable increase in the $K = 1$ strength, S_{31} , of the first $\xi = +1$ mode starting from zero at $\gamma = 0^\circ$. Let us examine the microscopic origin of this trend in more detail.

In Figs. 5 and 6, various quantities characterizing the lowest octupole modes with negative z -signature ($\alpha = -1$) at $\gamma = 4^\circ$ and $\gamma = 16^\circ$ are shown, respectively. These include the RPA forward and backward amplitudes, f_{ph} and g_{ph} , unperturbed particle-hole matrix elements of the octupole operator with $K = 1$, $O_{ph}^{(K=1,\xi)}$, and individual contributions to the RPA octupole transition amplitude, $M_{ph}^{(K=1,\xi)}$. Note that, although signs of f_{ph} , g_{ph} , and $O_{ph}^{(K=1,\xi)}$ depend on the chosen relative signs of single-particle wave functions, those of $M_{ph}^{(K=1,\xi)}$ are uniquely determined, because they are products of the former quantities. Thus, the relative signs of $M_{ph}^{(K=1,\xi)}$ between different particle-hole configurations serve as a good indicator of the coherence among them, and we can learn from their properties about the collectivity of the RPA mode under consideration. Therefore, in this figure, values of $M_{ph}^{(K=1,\xi)}$ are

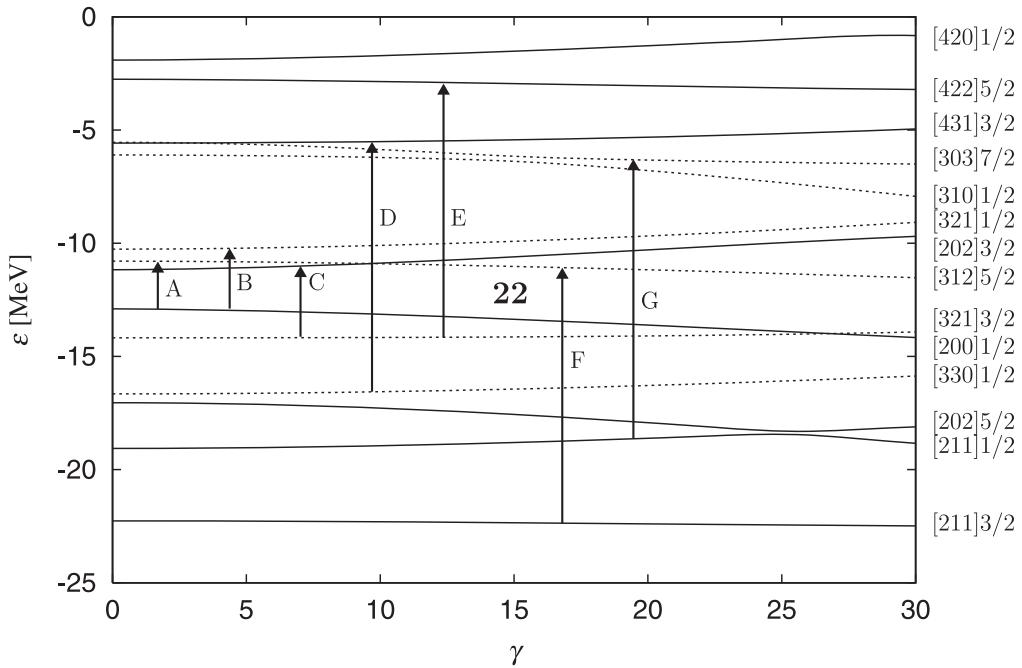


Fig. 4. Particle-hole configurations playing major roles in building up the lowest octupole vibrations with negative z -signature ($\alpha = -1$) (for both $\xi = \pm 1$). They are indicated by transition arrows with labels A, B, C, D, E, F, and G. The single-particle energies are plotted as functions of γ for a fixed value of $\beta = 0.5$. For convenience, they are labelled with asymptotic quantum numbers indicating the largest components at the prolate limit ($\gamma = 0^\circ$) and connected adiabatically for variation of γ . The arrows are drawn at arbitrary positions in γ . Positive and negative parity levels are indicated by solid and dotted lines, respectively. Note that only levels playing major roles in building up the lowest $\alpha = -1$ mode are explicitly drawn here; see Fig. 2 for a more complete single-particle diagram.

presented with their signs, while absolute values are shown for the other quantities. The $\gamma = 4^\circ$ case is chosen to examine the effect of incipient triaxial deformation on the octupole mode of interest and the $\gamma = 16^\circ$ case to represent typical triaxial deformation obtained in the SHF calculations.^{20),21)}

According to the bottom panel of Fig. 5, the particle-hole configurations, $[200]1/2 \rightarrow [321]1/2$ and $[321]3/2 \rightarrow [202]3/2$, labelled B and C, respectively (illustrated in Fig. 4), give the major contributions to the strength S_{31} of the lowest mode at $\gamma = 4^\circ$ for both modes with x -signature $\xi = \pm 1$. It should be noted that Fig. 5 applies to both protons and neutrons: in the $N = Z$ nucleus under consideration, proton and neutron excitations act coherently and markedly enhance the transition strengths. Thus, the proton and neutron contributions are summed up in the transition amplitude $M_{ph}^{(K=1,\xi)}$ (see their definition (3.19)).

We can notice some different properties between signature partners already at such a small triaxiality. The difference significantly develops at $\gamma = 16^\circ$ shown in Fig. 6. In fact, the octupole transition amplitude $M_{ph}^{(K=1,\xi)}$ associated with the

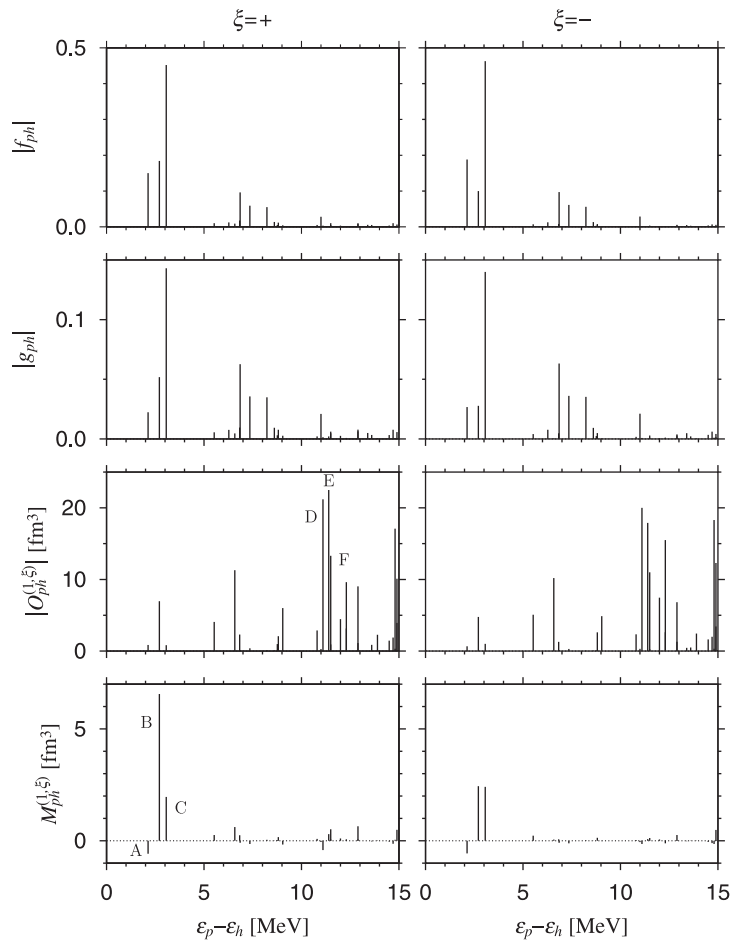


Fig. 5. Properties of the lowest octupole modes with negative z -signature ($\alpha = -1$) at the triaxiality parameter $\gamma = 4^\circ$. The result of calculation for the positive x -signature ($\xi = +1$) mode is displayed on the left-hand side, while that for the negative x -signature ($\xi = -1$) on the right-hand side. From the top to the bottom panels, RPA forward and backward amplitudes, f_{ph} and g_{ph} , unperturbed particle-hole matrix elements of the octupole operator with $K = 1$, $O_{ph}^{(K=1,\xi)}$, and individual contributions to the RPA octupole transition amplitude, $M_{ph}^{(K=1,\xi)}$, are displayed at positions of the abscissa axis representing unperturbed excitation energies, $\varepsilon_p - \varepsilon_h$, of individual particle-hole configurations composing the lowest RPA mode. Labels A, B, C, D, E, and F indicate some important configurations displayed in Fig. 4. Note that absolute values are shown except for $M_{ph}^{(K=1,\xi)}$. Note also that different scales are used for f_{ph} and g_{ph} .

configuration B, markedly increases for the positive x -signature mode ($\xi = +1$) but decreases for the negative x -signature mode ($\xi = -1$). Furthermore, higher-lying configurations, $[330]1/2 \rightarrow [431]3/2$, $[321]3/2 \rightarrow [422]5/2$, $[211]3/2 \rightarrow [312]5/2$, and $[211]1/2 \rightarrow [303]7/2$, respectively labelled D, E, F, and G (see Fig. 4), contribute appreciably only for the $\xi = +1$ mode. Note that they all contribute in the phase indicating that the collective character of the $\xi = +1$ mode is developed remarkably. In contrast, these contributions are much smaller for the $\xi = -1$ mode. This is the

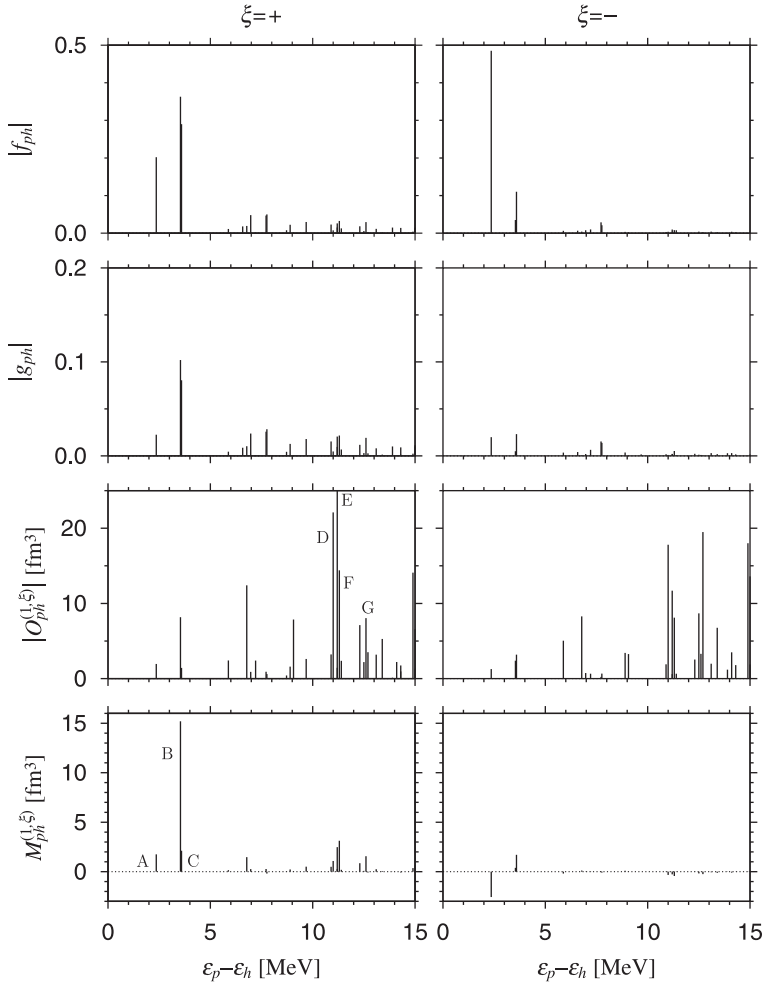


Fig. 6. Same as Fig. 5 but at the triaxiality parameter $\gamma = 16^\circ$. Note that different scales are used for g_{ph} and $M_{ph}^{(K=1,\xi)}$. The particle-hole excitation energy of configuration B is approximately the same with that of C.

microscopic origin of the striking difference of the octupole transition strength S_{31} between the lowest signature partners exhibited in Fig. 3.

4.3. Interplay of $K = 0$ and 2 components in the $\alpha = +1$ sector

In Fig. 7, we present the RPA excitation energies, octupole transition strengths with $K = 0$ and 2 (S_{30} and S_{32}) calculated for low-lying octupole excitation modes with positive z -signature ($\alpha = +1$) built on the SD state in ^{44}Ti as functions of triaxiality parameter γ . The lowest pair of excitation modes with $\xi = \pm 1$ has $K = 2$ in the prolate limit ($\gamma = 0^\circ$) and corresponds to the $K = 2$ doublet discussed in Ref. 21). As pointed out in that paper, appearance of this type of doublet pattern in excitation spectra may serve as a good indicator of triaxial deformation in the mean field. This signature-doublet possesses a large octupole strength S_{32} indicating

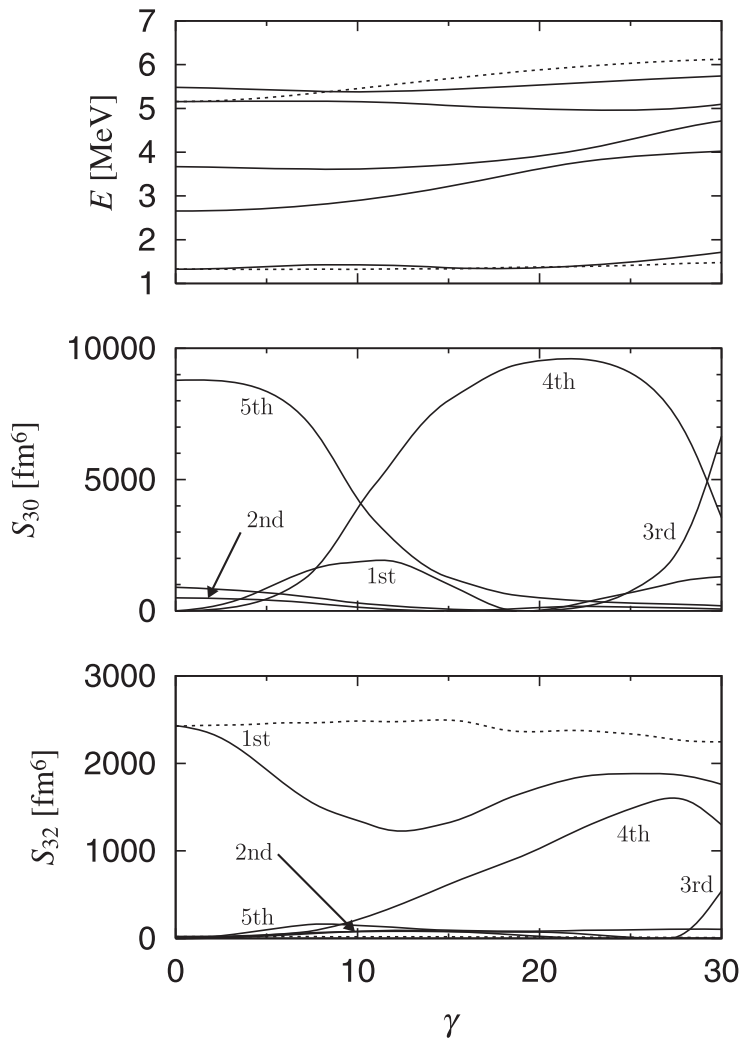


Fig. 7. Dependence on the triaxiality parameter γ of the RPA excitation energies (top panel), octupole transition strengths S_{30} ($K = 0$) (middle panel), and S_{32} ($K = 2$) (bottom panel), calculated for octupole excitation modes with positive z -signature ($\alpha = +1$) built on a superdeformed state in ^{44}Ti . The β is fixed at 0.5. Modes with negative x -signature ($\xi = -1$) are indicated by solid lines, while those with positive x -signature ($\xi = +1$) by dotted lines. Only the lowest five $\xi = -1$ modes are presented. Note that their signature partners with $\xi = +1$ exist only for the first and fourth modes which have $K = 2$ in the prolate limit.

their collective character. The main components of this doublet are the particle-hole excitations of protons and neutrons from the $[200]1/2$ level to the $[312]5/2$ level as illustrated with label H in Fig. 8, but coherent contributions of a large number of high-lying particle-hole excitations also play an indispensable role in generating collectivity of these lowest excitation modes.

The fourth pair of excitation modes, which exhibits a doublet pattern with

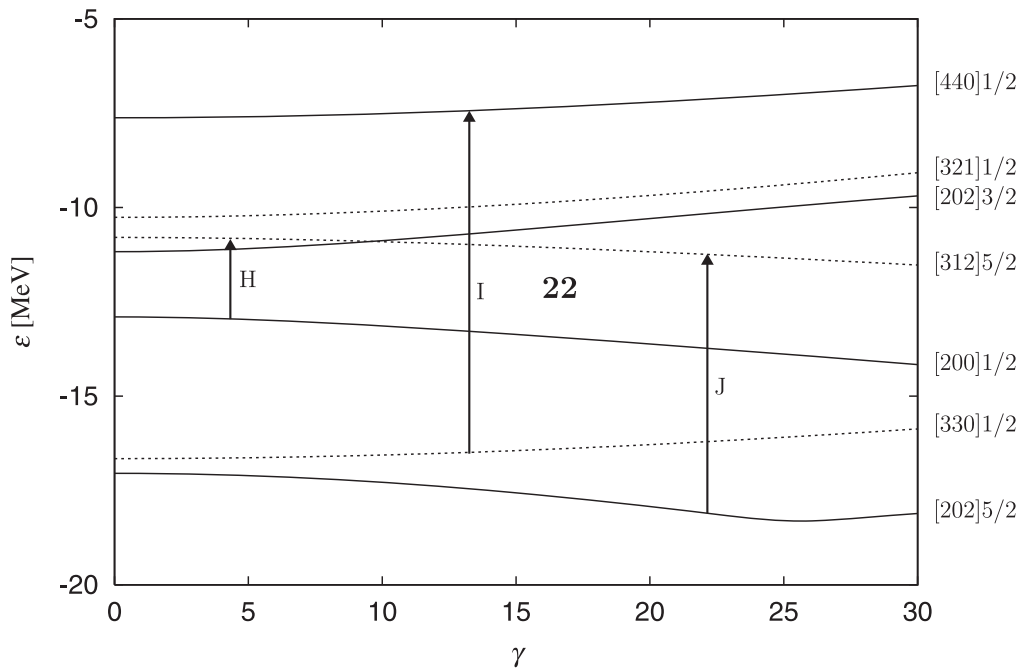


Fig. 8. Same as Fig. 4 but for the octupole vibrations with $(\alpha, \xi) = (+1, -1)$. Major particle-hole configurations are indicated by transition arrows with labels H, I, and J. Note that only levels playing major roles in building up the lowest $(\alpha, \xi) = (+1, -1)$ mode are explicitly drawn here; see Fig. 2 for a more complete single-particle diagram.

$\xi = \pm 1$ near the prolate limit, also has $K = 2$ there, but its S_{32} strength is very small indicating its noncollective character.

The second, third, and fifth excitation modes with $\xi = -1$ have $K = 0$ in the prolate limit, so that they have no x -signature partners. The $K = 0$ octupole strength S_{30} of the fifth mode is extremely large, indicating a strong collective character of this mode. On the other hand, the S_{30} strengths of the second and third modes are moderate. When the axial symmetry is broken, K -mixing takes place in the single-particle wave functions. Furthermore, the RPA modes that have different K quantum numbers (0 or 2) in the prolate limit start to interact with each other. Accordingly, x -signature splitting and K -mixing in the RPA modes develop with increasing γ . Thus, the $\xi = -1$ branch of the lowest excitation mode acquires an appreciable amount of the $K = 0$ octupole strength S_{30} in the region of $\gamma \simeq 5^\circ - 15^\circ$. Correspondingly, its S_{32} strength decreases in this region. In contrast, the S_{32} strength of its $\xi = +1$ partner stays almost constant because, as mentioned above, there is no $\xi = +1$ mode of $K = 0$ to mix with.

It is interesting to observe that a level crossing between the fourth and fifth modes slowly takes place in the region of $\gamma \simeq 10^\circ$. More precisely, because of the no crossing rule between the modes having the same quantum numbers, the two modes repel each other and exchange their characters when going through this region. This point is clearly seen in the plot of their S_{30} values. We note that this kind of interplay

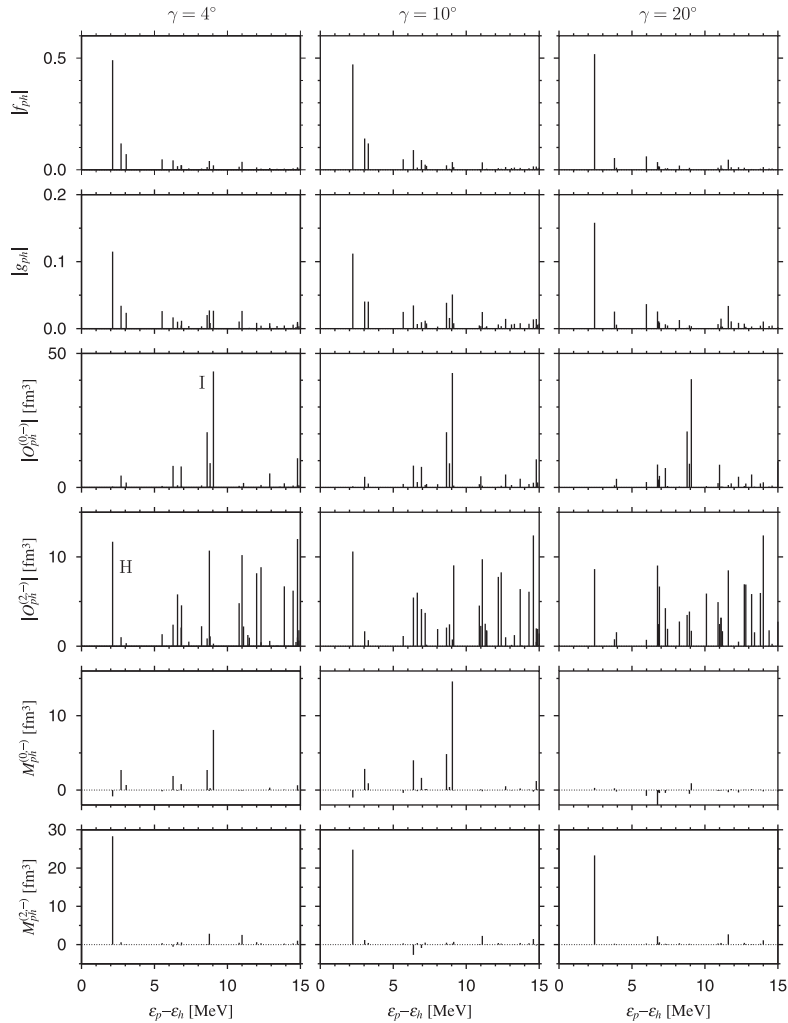


Fig. 9. Properties of the lowest octupole modes with $(\alpha, \xi) = (+1, -1)$. The results of calculation at the triaxiality parameter $\gamma = 4^\circ$, 10° , and 20° are presented on the left, middle, and right panels, respectively. From the top to the bottom panels, RPA forward and backward amplitudes, f_{ph} and g_{ph} , unperturbed particle-hole matrix elements of the octupole operators with $K = 0$ and $K = 2$, $O_{ph}^{(K=0,-)}$ and $O_{ph}^{(K=2,-)}$, and individual contributions to the RPA octupole transition amplitudes, $M_{ph}^{(K=0,-)}$ and $M_{ph}^{(K=2,-)}$, are displayed at positions of the abscissa axis representing unperturbed excitation energies, $\varepsilon_p - \varepsilon_h$, of individual particle-hole configurations composing the lowest RPA mode. Labels H and I indicate some important configurations displayed in Fig. 8. Note that absolute values are shown except for $M_{ph}^{(K=0,\xi)}$ and $M_{ph}^{(K=2,\xi)}$. Note also that different scales are used for f_{ph} and g_{ph} .

among a few $\xi = -1$ modes was not seen in the previous calculation.²¹⁾ The main cause of this difference is that, owing to slightly different single-particle energies, the lowest $K = 0$ mode and the other $K = 0$ modes are approximately separated in the latter calculation. This suggests that such detailed properties associated with

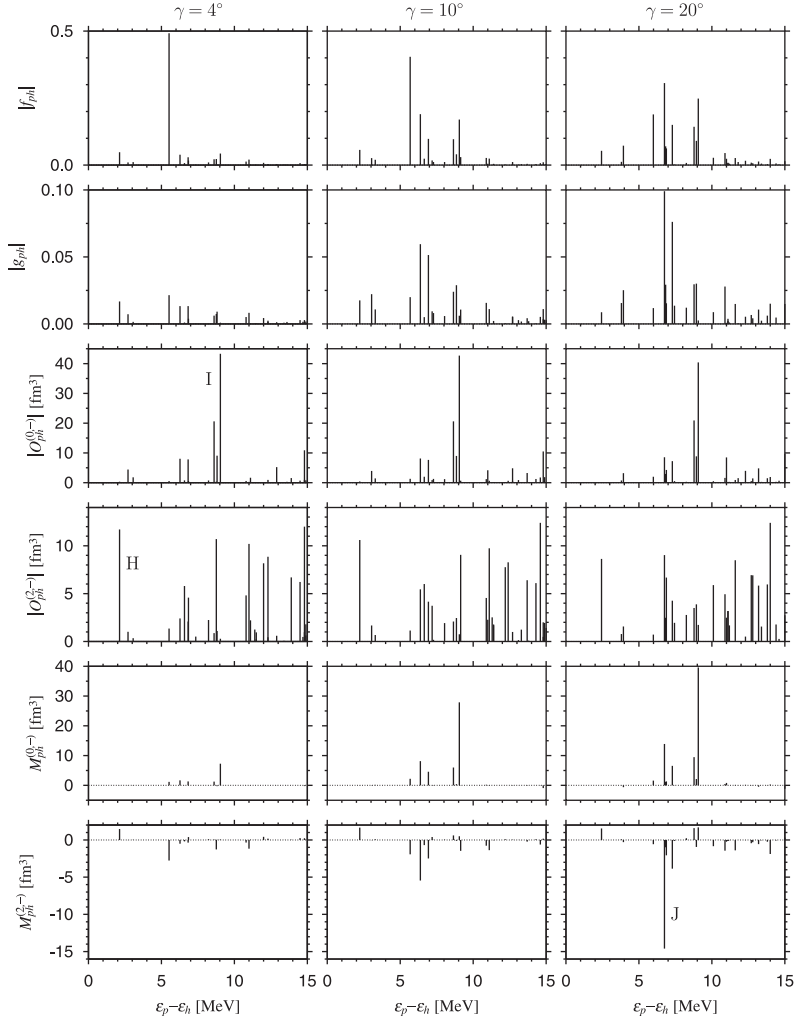


Fig. 10. Same as Fig. 9 but for the fourth excitation mode with $(\alpha, \xi) = (+1, -1)$.

interference among a few excitation modes are quite sensitive to the detailed shell structure of the mean field used in the RPA calculation.

We can investigate the microscopic origins of the γ dependence in the properties of excitation modes, exhibited in Fig. 7, by examining in detail the calculated RPA forward and backward amplitudes, f_{ph} and g_{ph} , unperturbed particle-hole matrix elements $O_{ph}^{(K,\xi)}$ of the octupole operators, and individual contributions $M_{ph}^{(K,\xi)}$ to the RPA octupole transition strengths. These quantities are displayed in Figs. 9 and 10 for the lowest and the fourth $\xi = -1$ modes, respectively. We again note that these figures apply to both protons and neutrons and their contributions are summed up in the transition amplitude $M_{ph}^{(K,\xi)}$. From Fig. 9, we learn that the increase in the S_{30} strength seen in Fig. 7 around $\gamma \simeq 10^\circ$ is associated with the mixture of the relatively high-lying particle-hole configuration, $[330]1/2 \rightarrow [440]1/2$ labelled I,

into this low-lying mode. This high-lying configuration corresponds to the excitation from the $f_{7/2}$ shell to the $g_{9/2}$ shell in the spherical limit and possesses an extremely large octupole matrix element $O_{ph}^{(0,-)}$. Therefore, its contribution to the transition amplitude $M_{ph}^{(0,-)}$ is large in spite of the fact that the RPA amplitudes, f_{ph} and g_{ph} , of this configuration are less than 0.1. In this manner, the low-lying collective RPA modes are generated by coherent superpositions of not only low-lying configurations but also many particle-hole configurations lying in the higher energy region.

In a similar manner, we can understand the reason why the S_{32} strength of the fourth mode increases in the region around $\gamma = 20^\circ$ by looking at Fig. 10. We see that the contribution to the transition amplitude $M_{ph}^{(2,-)}$ from the high-lying configuration, $[202]5/2 \rightarrow [312]5/2$, labelled J (see Fig. 8) markedly increases there. Note that, although these asymptotic quantum numbers are used for convenience to label the single-particle states, the z -component of angular momentum like $5/2$ is no longer a good quantum number under the triaxial deformation. In fact, the $[202]5/2$ level contains an appreciable amount of the $[200]1/2$ component so that the particle-hole configuration J possesses rather large $K = 2$ octupole matrix elements $O_{ph}^{(2,-)}$.

Finally, we point out another interesting trend seen in Fig. 7. The S_{30} strength of the lowest excitation modes is maximum in the region around $\gamma \simeq 10^\circ$ where the level crossing between the fourth and fifth excitation modes takes place, one of which carries an extremely large transition strength. Obviously, the mixing among these three modes is enhanced in this region. A similar trend is seen also near $\gamma = 30^\circ$ where the third and fourth excitation modes cross. Although we have not yet understood the deeper meaning of this result of calculation, it certainly indicates that the interplay of high-lying and low-lying particle-hole excitations plays an important role in generating collectivity of the low-lying octupole modes of excitation of interest.

§5. Concluding remarks

By means of the RPA calculation based on the triaxially deformed Woods-Saxon potential, we have investigated how axial-symmetry breaking in the mean field affects properties of the octupole vibrational excitations built on SD states in ^{44}Ti . By considering the magnitude of triaxial deformation γ as a parameter, detailed numerical analysis has been carried out with special attention to their dependence on signature quantum number with respect to rotation about an axis perpendicular to the longest axis by the angle of π . We have found a marked dependence of their properties on the signature quantum number.

Acknowledgements

We thank T. Inakura for giving us the result of the Skyrme-Hartree-Fock calculation to compare with our calculation result. The numerical calculations were carried out on supercomputers, NEC SX8 at the Yukawa Institute for Theoretical Physics in Kyoto University and NEC SX8R at the Research Center for Nuclear

Physics in Osaka University.

Appendix A

— Symmetry Properties of Single-Particle Wave Functions —

A.1. Reflection symmetries

The symmetry properties (2.12)–(2.14) are known^{26),27)} but we here summarize their proof because the ideas used here are further developed in the succeeding sections.

The relation (2.14) for reflection about the (x, y) -plane is obtained through the following manipulation:

$$\varphi_k(x, y, -z) = \mathcal{P}e^{i\pi\ell_z/\hbar}\varphi_k(x, y, z) \tag{A.1}$$

$$= e^{-i\frac{\pi}{2}\sigma_z}\mathcal{P}\mathcal{R}_z\varphi_k(x, y, z) \tag{A.2}$$

$$= -ip_k\alpha_k\sigma_z\varphi_k(x, y, z), \tag{A.3}$$

where the z -component of orbital angular momentum operator, ℓ_z , is replaced with $j_z - \frac{\hbar}{2}\sigma_z$.

The relation (2.13) for reflection about the (z, x) -plane is obtained through the following consideration. The eigenvalue equations (2.9)–(2.11) are invariant against the transformation $\mathcal{I} = \mathcal{K}\mathcal{P}e^{i\pi\ell_y/\hbar}$. As the eigenvalue for \mathcal{I} is ± 1 and the two equations, $\mathcal{I}\varphi_k(x, y, z) = \varphi_k(x, y, z)$ and $\mathcal{I}\{i\varphi_k(x, y, z)\} = -\{i\varphi_k(x, y, z)\}$ are apparently equivalent, we can choose the phase of our single-particle wave function satisfying the former relation without loss of generality. Since $\mathcal{I}\varphi_k(x, y, z) = \varphi_k^*(x, -y, z)$, Eq. (2.13) follows immediately.

With this phase convention, Eq. (2.9) for reflection about the (y, z) -plane is derived in the following manner:

$$\varphi_k(-x, y, z) = \mathcal{P}e^{i\pi\ell_y/\hbar}e^{i\pi\ell_z/\hbar}\varphi_k(x, y, z) \tag{A.4}$$

$$= e^{-i\frac{\pi}{2}\sigma_z}\mathcal{K}\mathcal{I}\mathcal{R}_z\varphi_k(x, y, z) \tag{A.5}$$

$$= -i\alpha_k\sigma_z\varphi_k^*(x, y, z). \tag{A.6}$$

A.2. Axially symmetric limit

In the prolate limit with $\gamma = 0^\circ$, the single-particle Hamiltonian $h(\vec{r}, \vec{\nabla})$ is symmetric about the z -axis, so that the single-particle wave functions $\varphi_k(\vec{r})$ can be written

$$\varphi_k(\vec{r}) = \begin{pmatrix} f_k(r, \theta)e^{i(m-\frac{1}{2})\phi} \\ g_k(r, \theta)e^{i(m+\frac{1}{2})\phi} \end{pmatrix}, \tag{A.7}$$

where $m\hbar$ is the angular momentum about the z -axis, and $f_k(r, \theta)$ and $g_k(r, \theta)$ possess the following symmetry properties for reflection about the (x, y) -plane: $f_k(r, \pi - \theta) = -ip_k\alpha_k f_k(r, \theta)$ and $g_k(r, \pi - \theta) = ip_k\alpha_k g_k(r, \theta)$.

Appendix B

— Symmetries of the A , B , and O Matrix Elements —

As we adopt the phase convention that the single-particle wave functions $\varphi_k(\vec{r})$ satisfy $\mathcal{I}\varphi_k(x, y, z) = \varphi_k(x, y, z)$, complex conjugation of these wave functions is equivalent to reflection about the (z, x) -plane ($\mathcal{K} = \mathcal{P}e^{i\pi\ell_y/\hbar}$), and time reversal is equivalent to symplectic transformation about the (z, x) -plane ($\mathcal{T} = \mathcal{PR}_y$). Also, there is a simple relation between the z -signature partner $\varphi_{\bar{k}}(\vec{r})$ and time-reversal partner $\mathcal{T}\varphi_k(\vec{r})$:

$$\varphi_{\bar{k}}(\vec{r}) = -i\alpha_k\mathcal{T}\varphi_k(\vec{r}). \quad (\text{B.1})$$

Using the above properties, we can prove that the RPA matrix elements possess the symmetries $A_{\bar{p}\bar{h}\bar{p}'\bar{h}'} = A_{php'h'}$ and $B_{\bar{p}\bar{h}\bar{p}'\bar{h}'} = B_{php'h'}$ through the following manner. These symmetries immediately follow from the corresponding symmetries of the matrix elements of the residual interaction $v_{\bar{k}'_1\bar{k}'_2\bar{k}_1\bar{k}_2}$, which are examined through the following manipulation:

$$\begin{aligned} v_{\bar{k}'_1\bar{k}'_2\bar{k}_1\bar{k}_2} &= \int \left[t_0 + \frac{1}{6}t_3\rho(\vec{r}) \right] \left\{ [\mathcal{T}\varphi_{k'_1}(\vec{r})]^\dagger [\mathcal{T}\varphi_{k_1}(\vec{r})] \right\} \left\{ [\mathcal{T}\varphi_{k'_2}(\vec{r})]^\dagger [\mathcal{T}\varphi_{k_2}(\vec{r})] \right\} d^3\vec{r} \\ &\quad + \int \left[t_0x_0 + \frac{1}{6}t_3x_3\rho(\vec{r}) \right] \left\{ [\mathcal{T}\varphi_{k'_1}(\vec{r})]^\dagger [\mathcal{T}\varphi_{k_2}(\vec{r})] \right\} \left\{ [\mathcal{T}\varphi_{k'_2}(\vec{r})]^\dagger [\mathcal{T}\varphi_{k_1}(\vec{r})] \right\} d^3\vec{r} \\ &= \int \left[t_0 + \frac{1}{6}t_3\rho(x, -y, z) \right] \\ &\quad \times \left[\varphi_{k'_1}^\dagger(x, -y, z)\varphi_{k_1}(x, -y, z) \right] \left[\varphi_{k'_2}^\dagger(x, -y, z)\varphi_{k_2}(x, -y, z) \right] d^3\vec{r} \\ &\quad + \int \left[t_0x_0 + \frac{1}{6}t_3x_3\rho(x, -y, z) \right] \\ &\quad \times \left[\varphi_{k'_1}^\dagger(x, -y, z)\varphi_{k_2}(x, -y, z) \right] \left[\varphi_{k'_2}^\dagger(x, -y, z)\varphi_{k_1}(x, -y, z) \right] d^3\vec{r} \\ &= v_{k'_1k'_2k_1k_2}. \end{aligned} \quad (\text{B.2})$$

In the first equality above, the relation $\varphi_{\bar{k}}(\vec{r}) = -i\alpha_k\mathcal{T}\varphi_k(\vec{r})$ is used. Note that $\alpha_{k'_1}^*\alpha_{k_1}\alpha_{k'_2}^*\alpha_{k_2} = +1$, because these are matrix elements between particle-hole pairs that carry a definite z -signature. In the second equality, the symmetry of the density, $\rho(x, -y, z) = \rho(x, y, z)$, and the relation, $\mathcal{T} = \mathcal{PR}_y$, are used as

$$\begin{aligned} [\mathcal{T}\varphi_{k'}(\vec{r})]^\dagger [\mathcal{T}\varphi_k(\vec{r})] &= [\mathcal{PR}_y\varphi_{k'}(x, y, z)]^\dagger [\mathcal{PR}_y\varphi_k(x, y, z)] \\ &= \varphi_{k'}^\dagger(x, -y, z)\varphi_k(x, -y, z). \end{aligned} \quad (\text{B.3})$$

In a similar fashion, we can prove the relations,

$$O_{hp}^{(K,\xi)} = -(-1)^K\xi O_{ph}^{(K,\xi)} \quad \text{and} \quad O_{\bar{p}\bar{h}}^{(K,\xi)} = -\xi O_{ph}^{(K,\xi)}, \quad (\text{B.4})$$

between particle-hole matrix elements of the Hermitian octupole operators $O^{(K,\xi)}(\vec{r})$ through the following steps:

$$O_{hp}^{(K,\xi)} = O_{ph}^{(K,\xi)*}$$

$$\begin{aligned}
 &= \int [\mathcal{K}\varphi_p(\vec{r})]^\dagger O^{(K,\xi)}(\vec{r}) [\mathcal{K}\varphi_h(\vec{r})] d^3\vec{r} \\
 &= \int [\mathcal{P}e^{-i\pi\ell_x/\hbar} e^{-i\pi\ell_z/\hbar} \varphi_p(\vec{r})]^\dagger O^{(K,\xi)}(\vec{r}) [\mathcal{P}e^{-i\pi\ell_x/\hbar} e^{-i\pi\ell_z/\hbar} \varphi_h(\vec{r})] d^3\vec{r} \\
 &= \int \varphi_p^\dagger(\vec{r}) e^{i\pi\ell_z/\hbar} e^{i\pi\ell_x/\hbar} \mathcal{P}^{-1} O^{(K,\xi)}(\vec{r}) \mathcal{P} e^{-i\pi\ell_x/\hbar} e^{-i\pi\ell_z/\hbar} \varphi_h(\vec{r}) d^3\vec{r} \\
 &= - \int \varphi_p^\dagger(\vec{r}) e^{i\pi\ell_z/\hbar} e^{i\pi\ell_x/\hbar} O^{(K,\xi)}(\vec{r}) e^{-i\pi\ell_x/\hbar} e^{-i\pi\ell_z/\hbar} \varphi_h(\vec{r}) d^3\vec{r} \\
 &= -\xi \int \varphi_p^\dagger(\vec{r}) e^{i\pi\ell_z/\hbar} O^{(K,\xi)}(\vec{r}) e^{-i\pi\ell_z/\hbar} \varphi_h(\vec{r}) d^3\vec{r} \\
 &= -(-1)^K \xi \int \varphi_p^\dagger(\vec{r}) O^{(K,\xi)}(\vec{r}) \varphi_h(\vec{r}) d^3\vec{r} \\
 &= -(-1)^K \xi O_{ph}^{(K,\xi)}, \tag{B.5}
 \end{aligned}$$

$$\begin{aligned}
 O_{\bar{p}\bar{h}}^{(K,\xi)} &= \int \varphi_{\bar{p}}^\dagger(\vec{r}) O^{(K,\xi)}(\vec{r}) \varphi_{\bar{h}}(\vec{r}) d^3\vec{r} \\
 &= (-1)^K \int [\mathcal{T}\varphi_p(\vec{r})]^\dagger O^{(K,\xi)}(\vec{r}) [\mathcal{T}\varphi_h(\vec{r})] d^3\vec{r} \\
 &= (-1)^K \int [\mathcal{P}\mathcal{R}_x^{-1}\mathcal{R}_z^{-1}\varphi_p(\vec{r})]^\dagger O^{(K,\xi)}(\vec{r}) [\mathcal{P}\mathcal{R}_x^{-1}\mathcal{R}_z^{-1}\varphi_h(\vec{r})] d^3\vec{r} \\
 &= (-1)^K \int \varphi_p^\dagger(\vec{r}) \mathcal{R}_z \mathcal{R}_x \mathcal{P}^{-1} O^{(K,\xi)}(\vec{r}) \mathcal{P} \mathcal{R}_x^{-1} \mathcal{R}_z^{-1} \varphi_h(\vec{r}) d^3\vec{r} \\
 &= -(-1)^K \int \varphi_p^\dagger(\vec{r}) \mathcal{R}_z \mathcal{R}_x O^{(K,\xi)}(\vec{r}) \mathcal{R}_x^{-1} \mathcal{R}_z^{-1} \varphi_h(\vec{r}) d^3\vec{r} \\
 &= -(-1)^K \xi \int \varphi_p^\dagger(\vec{r}) \mathcal{R}_z O^{(K,\xi)}(\vec{r}) \mathcal{R}_z^{-1} \varphi_h(\vec{r}) d^3\vec{r} \\
 &= -\xi \int \varphi_p^\dagger(\vec{r}) O^{(K,\xi)}(\vec{r}) \varphi_h(\vec{r}) d^3\vec{r} \\
 &= -\xi O_{ph}^{(K,\xi)}. \tag{B.6}
 \end{aligned}$$

In the above manipulation, use is made of the relations, $\mathcal{T} = \mathcal{P}\mathcal{R}_y$, $\varphi_{\bar{k}}(\vec{r}) = -i\alpha_k \mathcal{T}\varphi_k(\vec{r})$, $\alpha_p^* \alpha_h = (-1)^K$, $\mathcal{P}O^{(K,\xi)}(\vec{r})\mathcal{P}^{-1} = -O^{(K,\xi)}(\vec{r})$, $\mathcal{R}_z O^{(K,\xi)}(\vec{r})\mathcal{R}_z^{-1} = (-1)^K O^{(K,\xi)}(\vec{r})$ and $\mathcal{R}_x O^{(K,\xi)}(\vec{r})\mathcal{R}_x^{-1} = \xi O^{(K,\xi)}(\vec{r})$, together with identities,

$$e^{i\pi\ell_x/\hbar} e^{i\pi\ell_y/\hbar} e^{i\pi\ell_z/\hbar} = 1 \quad \text{and} \quad \mathcal{R}_x \mathcal{R}_y \mathcal{R}_z = \mathbf{1}. \tag{B.7}$$

References

- 1) P. J. Nolan and P. J. Twin, *Annu. Rev. Nucl. Part. Sci.* **38** (1988), 533.
- 2) S. Åberg, H. Flocard and W. Nazarewicz, *Annu. Rev. Nucl. Part. Sci.* **40** (1990), 439.
- 3) R. V. F. Janssens and T. L. Khoo, *Annu. Rev. Nucl. Part. Sci.* **41** (1991), 321.
- 4) C. Baktash, B. Haas and W. Nazarewicz, *Annu. Rev. Nucl. Part. Sci.* **45** (1995), 485.
- 5) C. Baktash, *Prog. Part. Nucl. Phys.* **38** (1997), 291.
- 6) J. Dudek, T. R. Werner and Z. Szymanski, *Phys. Lett. B* **248** (1990), 235.
- 7) J. Skalski, *Phys. Lett. B* **274** (1992), 1.
- 8) P. A. Butler and W. Nazarewicz, *Rev. Mod. Phys.* **68** (1996), 349.

- 9) M. Bender, P.-H. Heenen and P.-G. Reinhard, *Rev. Mod. Phys.* **75** (2003), 121.
- 10) S. Mizutori, Y. R. Shimizu and K. Matsuyanagi, *Prog. Theor. Phys.* **85** (1991), 559; *Prog. Theor. Phys.* **86** (1991), 131.
- 11) S. Mizutori, T. Nakatsukasa, K. Arita, Y. R. Shimizu and K. Matsuyanagi, *Nucl. Phys. A* **557** (1993), 125.
- 12) T. Nakatsukasa, K. Matsuyanagi, S. Mizutori and W. Nazarewicz, *Phys. Lett. B* **343** (1995), 19.
- 13) T. Nakatsukasa, K. Matsuyanagi, S. Mizutori and Y. R. Shimizu, *Phys. Rev. C* **53** (1996), 2213.
- 14) A. Korichi et al., *Phys. Rev. Lett.* **86** (2001), 2746.
- 15) D. Rossbach et al., *Phys. Lett. B* **513** (2001), 9.
- 16) T. Lauritsen et al., *Phys. Rev. Lett.* **89** (2002), 282501.
- 17) E. Ideguchi et al., *Phys. Rev. Lett.* **87** (2001), 222501.
- 18) C. J. Chiara et al., *Phys. Rev. C* **67** (2003), 041303.
- 19) C. D. O'Leary, M. A. Bentley, B. A. Brown, D. E. Appelbe, R. A. Bark, D. M. Cullen, S. Ertürk, A. Maj and A. C. Merchant, *Phys. Rev. C* **61** (2000), 064314.
- 20) T. Inakura, S. Mizutori, M. Yamagami and K. Matsuyanagi, *Nucl. Phys. A* **710** (2002), 261.
- 21) T. Inakura, H. Imagawa, Y. Hashimoto, S. Mizutori, M. Yamagami and K. Matsuyanagi, *Nucl. Phys. A* **768** (2006), 61.
- 22) A. Muta, J.-I. Iwata, Y. Hashimoto and K. Yabana, *Prog. Theor. Phys.* **108** (2002), 1065.
- 23) H. Imagawa and Y. Hashimoto, *Phys. Rev. C* **67** (2003), 037302.
- 24) K. Yoshida, M. Yamagami and K. Matsuyanagi, *Prog. Theor. Phys.* **113** (2005), 1251.
- 25) H. C. Pauli, *Phys. Rep.* **7** (1973), 35.
- 26) P. Bonche, H. Focard, P. H. Heenen, S. J. Kriger and M. S. Weiss, *Nucl. Phys. A* **443** (1985), 39.
- 27) P. Bonche, H. Focard and P. H. Heenen, *Nucl. Phys. A* **467** (1987), 115.
- 28) A. Bohr and B. R. Mottelson, *Nuclear Structure*, Vol. I (W. A. Benjamin Inc., 1969; World Scientific, 1998).
- 29) S. Shlomo and G. F. Bertsch, *Nucl. Phys. A* **243** (1975), 507.
- 30) A. Bohr and B. R. Mottelson, *Nuclear Structure*, Vol. II (W. A. Benjamin Inc., 1975; World Scientific, 1998).
- 31) P. Ring and P. Schuck, *The Nuclear Many-Body Problem* (Springer, 1980).
- 32) G. Colò, N. Van Giai, P. F. Bortignon and M. R. Quaglia, *Phys. Lett. B* **485** (2000), 362.